Protective effects of carbon dots derived from Rhei radix et rhizoma carbonisata on DSS (dextran sulfate sodium)-induced ulcerative colitis

Yifan Zhang
Beijing University of Chinese Medicine
Jie Zhao
Beijing University of Chinese Medicine
Yusheng Zhao
Beijing University of Chinese Medicine
Xue Bai
Beijing University of Chinese Medicine
Yumin Chen
Beijing University of Chinese Medicine
Yuhan Liu
Beijing University of Chinese Medicine
Yue Zhang
Beijing University of Chinese Medicine
Hui Kong
Beijing University of Chinese Medicine
Huihua Qu
Beijing University of Chinese Medicine
Yan Zhao (zhaoyandr@163.com)
Beijing University of Chinese Medicine

Research Article

Keywords: Rhei radix et rhizoma, carbon dots, ulcerative colitis, anti-inflammatory, antioxidant

Posted Date: April 28th, 2022

DOI: https://doi.org/10.21203/rs.3.rs-1587244/v1

Abstract

In this study, the protective effect of Rhei radix et rhizoma-based carbon dots (RRRC-CDs) on acute ulcerative colitis were investigated. The green high-temperature carbonization method is used to prepare novel RRRC-CDs. The morphology, structure, functional groups, and other information of RRR-CDs were captured by transmission electron microscope, high-resolution electron microscope, ultraviolet, fluorescence, Fourier transform infrared, X-ray photoelectron spectroscopy, and X-ray diffraction, and through pharmacodynamic experiments to studied the protective effect of RRRC-CDs on ulcerative colitis. The results demonstrated that the RRRC-CDs were almost spherical in diameter ranging from 1.374nm - 4.533nm, and composed of mainly C, N, and O. The RRRC-CDs inhibited DSS-induced inflammatory response and oxidative stress injury mainly by down-regulating TNF-α, IL-6, MPO, MDA and increasing the levels of IL-10, CAT, GSH, and SOD. RRRC-CDs showed a significant protective effect on ulcerative colitis. This study results indicated that RRRC-CDs have potential clinical application in ulcerative colitis.

Introduction

Carbon dots (CDs), known as carbon-based zero-dimensional fluorescent nanomaterials[1-2] with particle size range of about 10 nm, and a variety of organic functional groups are distributed on the spherical surface[3]. The CDs are highly praised by analytical researchers for their superior performance, including fluorescent properties, biocompatibility, low toxicity, and ease of functionalization. etc.[4-6]. Not only that, but CDs also show unexpected advantages in the field of biomedicine, such as targeted drug delivery, fluorescent probes, artificially simulated enzymes, photosensitizers, antibacterial molecular nanocarriers, etc[7-10]. Notably, the CDs extracted from traditional Chinese medicine (TCM), which have existed for thousands of years, have attracted more and more attention due to its environmental friendliness, abundant resources, and reproducibility [6].

A CD can be extracted from the process of high-temperature heating and carbonization of natural products to make charcoal drug (a kind of TCM preparation), similar to the "bottom-up" preparation process of CDs[11]. Based on this method, a variety of carbon drug have been prepared using a muffle furnace, making the preparation of carbon dots simple, fast, environmentally friendly, and mass-producible[12]. So far, carbon dots have been shown to have hemostatic activity[13-15], analgesic activity[16], anti-freeze injury[17], and more. Although there are many advantages, in terms of pharmacodynamics, the inherent differences of natural products also determine the differences of biological activities, which need to be further explored and studied.

The *Rhei radix et rhizoma* (RRR), named Da Huang in Chinese, the record of Da Huang as a medicine first appeared in *Shen Nong's Herbal Classic* more than 2,000 years ago. The Rhei Radix rhizoma carbonisata (RRRC) is the product of the carbonization of RRR. It has been recorded in ancient books that it has been used for the treatment of ulcerative intestinal diseases for thousands of years, for example, in 1922, the original text of *National Famous Traditional Chinese Medicine Cases Classification* recorded that fever

for one or two days, thirst and abdominal pain, from diarrhea to dysentery, tenesmus, mixed pus and blood, and the RRRC used in traditional Chinese medicine prescriptions. Its long-term application has proved the effectiveness and safety of RRRC. However, the biological activity of RRRC as a charcoal preparation has not been confirmed, and the material basis is still unclear yet.

UC, as a common clinical inflammatory enteritis of unknown origin, drug therapy is still the mainstream treatment. Drugs such as aminosalicylic acid, corticosteroids, and immunosuppressants are frequently used clinically. The short-term efficacy of these drugs is acceptable, but the long-term efficacy is unsatisfactory and causes serious side effects, such as thromboembolism and easy recurrence after discontinuation[18]. This searches for a safe, long-term, and effective therapeutic drug an urgent requirement. Therefore, based on the previous research of our team, we discovered RRRC, and we focused on the study of its active substances after carbonization, which was named RRRC-CDs, and evaluate the potential mechanism of RRRC-CDs protective effect on UC.

Materials And Methods

Chemicals

The RRR material was purchased from Beijing Qiancao Herbal Pieces Co., Ltd. (Beijing, China), and the RRRC was synthesized in a muffle furnace in our laboratory. Dialysis membranes (molecular weight cut-off was 1000 Da) were purchased from Beijing Ruida Henghui Technology Development Co., Ltd. (Beijing, China). Mouse SOD, MPO, MDA, GSH, CAT kits were brought from Nanjing Jiancheng Bioengineering Institute of China (Nanjing, China). Mouse IL-6, IL-10, TNF-α enzyme-linked immunosorbent assay (ELISA) kits were brought from Cloud-Clone Crop. (Wuhan, China). The cell counting kit-8 (CCK-8) was brought from Dojindo Molecular Technologies, Inc. (Kumamoto, Japan). All other chemicals and reagents were of analytical grade. De-ionized water was employed throughout this study.

Animals

All research complied with the Guide for the Care and Use of Laboratory Animals and approved this Ethics Review Committee for Animal Experimentation at the Beijing University of Chinese Medicine. Male BALB/C mice (weighing 22.0g±2.0g) were obtained from Beijing Vital River Laboratory Animal Technology Co., Ltd (Beijing, China). The animals were housed in a well-ventilated room temperature of 24.0 ± 1.0℃ with 55 – 65% relative humidity under a 12h light/dark cycle. Access to food and water was unlimited.

Preparation of RRRC-CDs

The RRRC-CDs were prepared in the muffle furnace (TL0612 muffle furnace, Beijing Zhong Ke Aobo Technology Co., Ltd, Beijing, China) by one-step pyrolysis. First, the RRR samples were placed in separated crucibles, covered with aluminum foil paper with sealed lids. Then the RRR was carbonized in a pre-heated muffle furnace at 350℃ for 1h. After cooling to room temperature, the RRR was ground to a

fine powder and boiled twice in the water bath at 100℃ for 1h per time. Whereafter, the decoction solution was filtered (0.22μm microfiltration membrane), concentrated, and dialyzed (1000 Daltons molecular weight cut-off dialysis membrane). The obtained RRRC-CDs were stored at 4℃ until further use. The preparation flow chart of RRRC-CDs is shown in Figure 1.

Characterization of RRRC-CDs

The morphology, particle size distribution, microstructure information of RRRC-CDs were characterized by transmission electron microscopy (TEM, Tecnai G220, FEI Company, Hillsboro, OR, USA) with electron energy of 200 kV. Atomic lattice spacing and other internal details were examined using HRTEM with a JEN-1230 (Japan Electron Optics Laboratory, Japan). Through an X-ray photoelectron spectrometer (XPS), the surface composition of the sample was analyzed using an ESCALAB 250Xi XPS (Thermo Fisher Scientific, MA, USA) with a monochromatic Al Kα x-ray source. The spectral properties of the CDs were recorded by the ultraviolet spectrophotometer (CECIL, Cambridge, UK) and by the fluorescence spectrophotometer (F-4500, Hitachi, Tokyo, Japan). Additionally, the Fourier-transform infrared (FTIR) spectroscopy was characterized with FTIR spectrophotometer (spectral window between 400 and 4000 cm^{-1}, Thermo Fisher, CA, USA). X-ray diffraction (XRD, D8 Venture Plus X-ray Diffractometer, Bruker AXS, Karlsruhe, Germany) was measured with Cu K-alpha radiation.

In vitro cytotoxicity: CCK-8 assay

The cytotoxicity of RRRC-CDs was detected by CCK-8 assay. The RAW 264.7 cells were cultured in DMEM medium containing 20% fetal bovine serum in a humidified 5% CO2 atmosphere at 37°C. First, the cells were seeded into 96-well plates at a density of 2×10^5 cells per well and incubated for 12 hours. Following this, the original medium was abandoned in each well, and RRRC-CDs with different concentrations (1000 μg/mL, 500 μg/mL, 250 μg/mL, 125 μg/mL, 62.5 μg/mL, 31.25 μg/mL, 15.625 μg/mL) was added for further incubation for 24 hours. After 24 h, washed with phosphate buffered saline (PBS) to remove all the culture medium in the 96-well plates, and then 10 μL/well CCK-8 solution and 100 μL/well medium was added to incubate for an additional 2 h. The pure DMEM as a blank and the absorbance of each well was detected by a microplate reader (Biotek, VT, USA) at 450nm wavelength. Untreated cells were used as the control. The cell viability calculation formula is as follows.

Cell viability (% of control) = (Ae− Ab / Ac− Ab) × 100

Ae, Ab and Ac correspond to the absorbance of experimental group, blank group and control group respectively.

Model of UC and drug treatment

Free drinking of 4% DSS water solution for 7 days to establish acute ulcerative colitis model. BALB/C male mice (7 weeks old, n=36) were randomly divided into six groups:the control group (normal saline [NS] 10 mL/kg), model group ([NS] 10 mL/kg), positive group (salazosulfadimidine [SASP] 500 mg/kg),

high-dose group (RRRC-CDs 0.23 mg/kg), medium-dose group (RRRC-CDs 0.12 mg/kg) and low-dose group (RRRC-CDs 0.06 mg/kg). Only the control group drank pure water freely per day, and all the other groups drank 4% DSS aqueous solution freely.

The mice were sacrificed on the second day after the modeling was completed. The blood and colon tissues were collected to access the macroscopic and histopathological changes.

Disease activity index

Throughout the study, we observed the weight, activity, mental state, stool characteristics, and mortality of the mice daily, and scored the disease activity index according to the weight, stool shape, and occult blood, as shown in Table 1.

Table 1 Disease activity index**

Score	Weight loss(%)*	Stool shape	Occult/grave blood
0	0	Normal	Negative
1	1-5	Loose stool	-
2	5-10	Loose stool	Hemoccult positive
3	10-15	Diarrhea	-
4	>15	Diarrhea	Grave blood

* : Based on the weight before modeling, Percentage weight loss = (Basal body weight (g) - daily mice body weight (g)) / basal body weight (g) × 100%

** : Disease activity index = (percentage weight loss + stool shape score + occult/grave blood score) / 3.

Histopathological Evaluation

After the colon tissue was observed and photographed, part of the colon tissue was quickly fixed in 4% paraformaldehyde solution, dehydrated, embedded in paraffin, and stained with hematoxylin and eosin (H&E). Observe and record the stained sections with a microscope at 200x and 400x.

Detection of Relevant Biochemical Indicators and inflammatory factors in Colon Tissues

The remaining colon tissue was washed with pre-cooled saline (0.9%) and cut into small pieces and homogenized with pre-cold saline. Then, one part was directly applied with suspension, and the other part was centrifuged at 3000 rpm for 10 min to gain the supernatant, which was used to test the level of inflammatory factors (TNF-α, IL-6, IL-10) and oxidative stress (MOP, MDA, SOD, GSH, CAT). All the procedures were carried out by the instructions.

Statistical Analysis

The results were performed by using IBM SPSS Statistics (version 20, SPSS Inc., Chicago, IL, USA). For data with normal distribution and homogeneity of variance, the mean ± standard deviation is provided. One-way analysis of variance (ANOVA) was used to compare differences between groups. Non-normally distributed data were analyzed by nonparametric statistical analysis using the Kruskal-Wallis test. $p<0.05$ and $p<0.01$were considered statistically significant differences.

Results

Characterization of RRRC-CDs

The TEM and HRTEM images of RRRC-CDs obtained at 350℃ for 1h and analyzed the morphology and particle size distribution of RRRC-CDs (Figure 2A, D). The TEM image shows that the RRRC-CDs were nearly spherical, which particle size distribution was concentrated range of 1.374nm - 4.533nm and the distribution was uniform. HRTEM images of the RRRC-CDs indicated that the lattice distance of RRRC-CDs was 0.132 nm.

The UV-Vis absorption spectrum revealed that RRRC-CDs had a broad spectrum without clear peaks (Fig. 2C). RRRC-CDs showed maximum fluorescence emission at 436 nm upon excitation at 321 nm (Figure 2E).

The surface chemical characteristics of CDs were characterized by FTIR spectroscopy (Figure 2F). The strong characteristic absorption peak at 3446.18 cm^{-1} may be the stretching vibration peak of -OH. The absorption peaks at 2918.51 cm^{-1} and 2850.34 cm^{-1} correspond to -CH_2- stretching. RRRC-CDs showed a C=O absorption peak at 1635.12 cm^{-1}. At 1384.29 cm^{-1}, the absorption peak may be the in-plane bending vibration peak of -OH or the stretching vibration peak of the C-N bond. The position of 1111.15 cm^{-1} was the absorption peak of C-O-C, which indicate the existence of the C-O-C bond.

The wide-angle XRD pattern in Figure 1B shows that there is a diffraction peak at about $2\theta = 23.5°$, which is in good agreement with the lattice parameters of RRRC-CDs.

The XPS was used to obtain the surface element composition and micro-chemical environment of RRRC-CDs. As shown in Figure 3A, The CDs contain three main peaks of C (67.99%), O (28.36%), and N (3.33%), which correspond to 284.9, 531.76, and 399.72 eV of the spectrum respectively. In addition, there is a trace amount of S (0.01%). The C1s spectrum of RRRC-CDs given in Figure 3B could be divided into three component peaks: 285.21 eV (C-N), 284.38 eV (C-C/C=C), and 287.96 eV (C-N/C-O) [11, 16]. The high-resolution O1s (Figure 3C) mainly contained two sub-peaks corresponding to 531.28 eV (C-O) and 532.52 eV (C-OH) [19,20]. In addition, the two peaks 399.9 and 399.09 eV [20,12] in the N1s spectrum (Figure32D) confirmed the existence of C-N-C and N-H bonds.

Histogram of particle size distribution. (B) XRD pattern. (C) Ultraviolet visible specturm. (D) High-resolution transmission electron microscope image. (E) Excitation and emission fluorescence spectra. (F) Fourier transform infrared spectroscopy.

Toxicity evaluation of RRRC-CDs

The experimental results (Figure 4) evaluated that the RRRC-CDs still did not show cytotoxicity at concentrations up to 1000 μg/mL, but instead had a little effect of promoting cell proliferation.

RRRC-CDs Alleviated DSS-Induced ulcerative colitis in Rats

The experimental time schedule of DSS-induced acute ulcerative colitis was established as shown in Figure 5A. DSS-induced colitis is mainly manifested by obvious weight loss, diarrhea, bloody stool, and other symptoms. In this study, it was found that the model group experienced significant weight loss compared to the control group, However, the RRRC-CDs high-, medium-, low-dose group modulated weight loss in mice during the disease, as shown in Figure 5B. At the same time, the DAI score is the severity of colitis commonly used evaluation index. The study found that the DAI score of the model (2.83 ± 0.40) group was extremely increased after DSS intake, and RRRC-CDs (H: 1.89 ± 1.06, $p<0.01$, M:1.22 ± 0.17, $p<0.01$, L: 1.94 ± 0.57, $p<0.01$) dramatically decreased the DAI score of experimental colitis (Figure 5C). Colon shortening is often associated with this disease, and RRRC-CDs has a sensibly inhibitory effect on colon shortening, as shown in Figure 5D-E.

RRRC-CDs Ameliorated DSS-Induced colitis Histopathological Damage

H&E staining was performed on different groups to explore the histopathological features of the colon, revealing DSS-induced damage and the protective biological activity of RRRC-CDs, as shown in Figure 6. The sections clearly showed that the colon tissue mucosa in the control group (Figure 6A) was intact, the mucosal cells were neatly arranged, and there was no inflammatory cell infiltration. In contrast, in the DSS-induced model group (Figure 6B), the colon tissue mucosal structure was incomplete, the crypts partially disappeared, and the mucosal inflammatory cell infiltration was obvious. After RRRC-CDs treatment, colon tissue in the RRRC-CDs groups (Figure 6C-F) was significantly protected. Among them, the mucosal structure of the RRRC-CDs medium group (Figure 6E) was close to normal, the cells were arranged neatly, and the infiltration of inflammatory cells was less.

Effect of RRRC-CDs on the levels of inflammatory cytokines in colon tissue

The effect of RRRC-CDs on the levels of inflammatory cytokines in the colon was evaluated by measuring the levels of TNF-α, IL-6, and IL-10 in colon tissue, as shown in Figure 7A-C. Compared with the control group (6.83 ± 1.17 ng/mL), the content of TNF-α in the colon tissue of the model group (12.25 ± 2.10 ng/mL) was increased ($p<0.01$). Compared with the model group, the content of TNF-α in the colon tissue of mice in the SASP (9.93 ± 2.76 ng/mL) and the RRRC-CDs (H: 9.86 ± 1.28 ng/mL, M: 7.95 ± 2.43 ng/mL, L: 9.21 ± 3.32 ng/mL) group showed a decreasing trend, and the difference between the RRRC-CDs medium and low groups was statistically significant (M: $p<0.01$, L: $p<0.05$).

The content of IL-6 in the tissue detected by ELISA (Figure 7B). It can be seen that the IL-6 was significantly activated in the model (1.88 ± 0.23 ng/mL) group drinking DSS compared to the control (0.75 ± 0.11 ng/mL) group drinking pure water ($p<0.01$). However, the level of IL-6 decreased in the RRRC-

CDs (H: 0.91 ± 0.21 ng/mL, p<0.01, M: 0.80 ± 0.31 ng/mL, p<0.01, L: 1.35 ± 0.27 ng/mL, p<0.01) treatment group and SASP (1.11 ± 0.32 ng/mL) group, and there were significant statistical differences.

In addition, Figure 7C presents the concentration of IL-10 in mouse colon tissue. Compared with the control (5.01 ± 1.54 ng/mL) group, the model (2.30 ± 0.89 ng/mL) group showed a significant decrease (p<0.01), and the SASP (3.20 ± 0.4 ng/mL) group and the RRRC-CDs (H: 3.68 ± 0.65 ng/mL, M: 4.50 ± 1.51 ng/mL, L: 3.45 ± 1.70 ng/mL) group showed an upward trend, of which the high-dose (p<0.05) group and the middle-dose (p<0.01) group increased significantly, while the SASP group and the low-dose group increased IL-10 concentrations, but no significant difference (p>0.05).

Effect of RRRC-CDs on the levels of oxidative stress in colon tissue

To further verify the protective effect of RRRC-CDs on ulcerative colitis, the antioxidant capacity was measured by the content of enzyme antioxidant (CAT, SOD) and non-enzyme antioxidant (GSH) in intestinal tissues (Figure 8A-C). Intestinal tissue damage caused by oxidative stress was assessed by the levels of MDA and MPO (Figure 8D and E). After DSS intake, MPO and MDA contents in the intestinal canal of mice in the model (MPO: 0.29 ± 0.10 U/g, p<0.01, MDA: 29.83 ± 5.75 U/mgprot, p<0.01) group increased sharply compared with the control (MPO: 0.07 ± 0.03 U/g, MDA: 12.16 ± 2.19 U/mgprot) group. In contrast, the RRRC-CDs (MPO: H: 0.12 ± 0.03 U/g, p<0.01, M: 0.08 ± 0.01 U/g, p<0.01, L: 0.12 ± 0.03 U/g, p<0.01, MDA: H: 20.33 ± 5.47 U/mgprot, p<0.01, M: 17.16 ± 1.95 U/mgprot, p<0.01, L: 24.00 ± 4.93 U/mgprot, p<0.05) administration group largely inhibited intestinal damage caused by peroxide.

Figure 8A shows SOD activity values in each group. The contents of SOD in the colon tissue of mice in the model (64.23 ± 9.68 U/mgprot) group was significantly reduced (p<0.01), while SOD activity in the positive (98.40 ± 25.09 U/mgprot, p<0.05) group and RRRC-CDs high- (99.81 ± 24.68 U/mgprot, p<0.05), medium- (115.46 ± 23.00 U/mgprot, p<0.01), and low- (96.20 ± 18.83 U/mgprot, p<0.05) dose groups was increased to varying degrees, especially in the medium-dose group (p<0.01).

Similarly, the content of CAT and GSH in colon tissue exhibited consistent results (Figure 8B-C). After ingesting DSS solution, the content of model group decreased significantly (CAT: 7.45 ± 0.70 U/mgprot, p<0.01, GSH: 21.16 ± 3.50 mg/gprot, p<0.01) compared with control group (CAT: 13.80 ± 0.99 U/mgprot, GSH: 66.05 ± 7.03 mg/gprot). After treatment with positive drugs (CAT: 9.32 ± 1.26 U/mgprot, p<0.01, GSH: 37.42 ± 11.21 mg/gprot) and RRRC-CDS (CAT: H: 10.05 ± 0.89 U/mgprot, p<0.01, M: 11.92 ± 1.50 U/mgprot, p<0.01, L: 9.41 ± 0.53 U/mgprot, p<0.01, GSH: H: 41.97 ± 12.06 mg/gprot, p<0.01, M: 51.60 ± 7.44 mg/gprot, p<0.01, L: 40.78 ± 5.79 mg/gprot, p<0.01), the contents of CAT and GSH were significantly reversed.

Discussion

Ulcerative colitis (UC), first named by Samuel Wilks in 1859[21], is a chronic, relapsing disease that begins with inflammation of the rectal mucosa, continues to invade the submucosa on the one hand, and extends proximally on the other hand until it involves all parts of the whole large intestine[22]. Once sick,

patients often suffer from clinical symptoms such as abdominal pain, pus, and blood in the stool, tenesmus, weight loss, and so on. The pathogenesis of ulcerative colitis is still inconclusive, and there are various pathogenic factors. It is currently believed to be related to genetic factors, environmental changes, intestinal microbes, and immune factors[23]. Among them, UC is driven by inflammation caused by an increase in various pro-inflammatory factors secreted by different cell types[24]. Safe and effective drugs have yet to be developed to improve the clinical dilemma.

Researchers at home and abroad are increasingly hot on the nanomaterials, because of its excellent photobleaching resistance[25], photochemical stability[26], low toxicity[27], and other characteristics, and the CDs begin to become a new generation of nanoinnovative materials to occupy an important market. Existing research reports[28] suggest that the research on CDs is mostly from the perspective of nanocarriers and inherent biological activities. For example, doxorubicin-loaded polymer-coated carbon nanodots can pass through the blood-brain barrier and realize the pH-responsive sustained release of doxorubicin enables chemotherapeutic drug delivery into the brain[29]. In addition, the anti-inflammatory activity of aspirin-based carbon dots has been demonstrated[30]. Nevertheless, the current development of bioactivity for CD is relatively narrow, which may be concerned with the absence of intrinsic bioactivity of the raw materials or the lack of raw materials with rich carbon sources.

The preparation method of CDs also plays a crucial role in the development of the biological activity. With the deepening of the research on CDs, the disadvantages of the preparation methods of CDs are gradually exposed, for its arc discharge, chemical oxidation, hydrothermal[31], etc, which require strong acid and complex process. The improved high-temperature pyrolysis method meets the preparation requirements of low cost, easy operation, low toxicity, and environmental-friendly. It is worth noting that this preparation process for RRRC similar with CDs[32], so this study speculated that the active ingredient of RRRC may be CDs generated during the high-temperature heating process. The high-temperature carbonization of *Phellodendri Chinensis Cortex, Mulberry silkworm cocoon*, and *Lonicerae japonicae Flos* has been reported in the previous literature reports. [22, 33, 34].

In recent years, TCM has become increasingly active in the field of nanomaterials as part of the Chinese medical system. For example, *Glycyrrhizae Radix et Rhizoma* (GRR) Carbonisata with GRR as a precursor has been shown the anti-gastric ulcer activity[35], and *Paeoniae Radix Alba*-based CDs have liver-protecting activity[36], etc. The RRRC-CDs studied in this paper described a new type of carbon-based nanoparticles with a size distribution ranging from 1.374nm to 4.533nm prepared from the natural product RRR as the carbon source.

More importantly, for the first time, this study demonstrated the protective effect of RRRC-CDs against DSS-induced ulcerative colitis. As a chemical E. coli with anticoagulant properties, DSS induces a model of ulcerative colitis most similar to human UC, but its modeling mechanism is unclear and may be concerned with damage to the epithelial layer in the large intestine[37]. In fact, after ingesting DSS, mice gradually showed weight loss and increased DAI index. After treatment with RRRC-CDs, the weight loss of

mice was slowed down and the DAI score was significantly reduced. As an indirect indicator, RRRC-CDs markedly improved Colon shortening caused by DSS.

The inflammatory response is an important factor in the initiation, progression, and aggravation of UC. Cell-signaling molecules drive inflammation by generating inflammatory mediators or activating inflammatory pathways, allowing cytokines to damage the intestinal epithelium and barrier system directly[20]. Previous studies have confirmed[38] that down-regulation of downstream pro-inflammatory cytokines (such as TNF-α, IL-6, etc.) or up-regulation of anti-inflammatory cytokines (such as IL-10) can improve colonic injury of UC. This study confirmed that oral RRRC-CDs downregulated the levels of TNF-α, IL-6, and IL-10 and further alleviated the progressive aggravation of colon tissue, which may be one of the potential mechanisms by which RRRC-CDs protects colon tissue.

Oxidative damage mediated by overexpressed reactive oxygen species (ROS) is another crucial mechanism of UC. Sustained production of ROS may continuously deplete endogenous antioxidants, leading to lipid peroxidation and aggravating colonic damage[39]. Inhibiting the production of oxidants such as lipid peroxides or increasing the levels of antioxidants can attenuate DSS-induced colon damage[40]. The above results indicated that RRRC-CDs significantly inhibited the contents of MPO and MDA and increased the activity of SOD, CAT, GSH, which may be the underlying mechanism of RRRC-CDs to alleviate colon injury.

This study verified the protective effect of RRRC-CDs on DSS-induced ulcerative colitis from two aspects of inflammatory factors and oxidative stress and explained the potential mechanism, but further examinations are demanded to expose the deeper mechanisms of these effects.

Conclusion

In summary, this study uses the natural product RRR as the carbon source to synthesize and identify RRRC-CDs, which with an excellent biological activity using a one-step pyrolysis method. And for the first time, it was demonstrated that RRRC-CDs have a protective effect on ulcerative colitis from the aspects of inflammation and oxidative stress. The potential mechanism of RRRC-CDs was related to downregulation of downstream pro-inflammatory factors and upregulation of anti-inflammatory factors, as well as inhibition of lipid peroxidation and enhancement of scavenging capacity of oxygen free radicals. This study provides a new idea for the drug development of ulcerative colitis disease and also provides a new vision for the flexible use of clinical drugs.

Declarations

Ethics approval and consent to participate

All research complied with the Guide for the Care and Use of Laboratory Animals and approved this Ethics Review Committee for Animal Experimentation at the Beijing University of Chinese Medicine.

Consent for publication

Agree to publish without any conflict of interest.

Availability of Data and Materials

All data generated or analysed during this study are included in this published article.

Competing interests

The author declare no competing interest.

Funding

This work was supported by the Special Funds for Fundamental Research Funds of institutions of higher-learning affiliated with central departments. (grant number 2019-JYB-TD-001)

Authors' Contributions

Yifan Zhang, Yan Zhao and Huihua Qu designed the research. Yifan Zhang, Jie Zhao, Yumin Chen, Xue Bai, Yuhan Liu performed the research. Hui Kong and Yue Zhang analysed the data. Yusheng Zhao and Jie Zhao co-wrote the paper.

Acknowledgements

The authors thank all members of our laboratory for their useful comments and discussions.

References

1. Alaghmandfard, A., Sedighi, O., Tabatabaei Rezaei, N., Abedini, A. A., Malek Khachatourian, A., Toprak, M. S., Seifalian, A., Recent advances in the modification of carbon-based quantum dots for biomedical applications. *Mater Sci Eng C Mater Biol Appl* **2021,** *120*, 111756.
2. Zhao, D. L., Chung, T. S., Applications of carbon quantum dots (CQDs) in membrane technologies: A review. *Water Res* **2018,** *147*, 43-49.
3. Kang, Z., Lee, S. T., Carbon dots: advances in nanocarbon applications. *Nanoscale* **2019,** *11* (41), 19214-19224.
4. Cohen, E. N., Kondiah, P. P. D., Choonara, Y. E., du Toit, L. C., Pillay, V., Carbon Dots as Nanotherapeutics for Biomedical Application. *Curr Pharm Des* **2020,** *26* (19), 2207-2221.
5. Miao, H., Wang, L., Zhuo, Y., Zhou, Z., Yang, X., Label-free fluorimetric detection of CEA using carbon dots derived from tomato juice. *Biosens Bioelectron* **2016,** *86*, 83-89.
6. Zhang, X., Jiang, M., Niu, N., Chen, Z., Li, S., Liu, S., Li, J., Natural-Product-Derived Carbon Dots: From Natural Products to Functional Materials. *ChemSusChem* **2018,** *11* (1), 11-24.

7. Nair, A., Haponiuk, J. T., Thomas, S., Gopi, S., Natural carbon-based quantum dots and their applications in drug delivery: A review. *Biomed Pharmacother* **2020,** *132*, 110834.
8. Purbia, R., Paria, S., A simple turn on fluorescent sensor for the selective detection of thiamine using coconut water derived luminescent carbon dots. *Biosens Bioelectron* **2016,** *79*, 467-75.
9. Devi, P., Saini, S., Kim, K. H., The advanced role of carbon quantum dots in nanomedical applications. *Biosens Bioelectron* **2019,** *141*, 111158.
10. Bharathi, D., Siddlingeshwar, B., Krishna, R. H., Singh, V., Kottam, N., Divakar, D. D., Alkheraif, A. A., Green and Cost Effective Synthesis of Fluorescent Carbon Quantum Dots for Dopamine Detection. *J Fluoresc* **2018,** *28* (2), 573-579.
11. Yue, L., Li, H., Liu, Q., Guo, D., Chen, J., Sun, Q., Xu, Y., Wu, F., Manganese-doped carbon quantum dots for fluorometric and magnetic resonance (dual mode) bioimaging and biosensing. *Mikrochim Acta* **2019,** *186* (5), 315.
12. Kirbas Cilingir, E., Seven, E. S., Zhou, Y., Walters, B. M., Mintz, K. J., Pandey, R. R., Wikramanayake, A. H., Chusuei, C. C., Vanni, S., Graham, R. M., Leblanc, R. M., Metformin derived carbon dots: Highly biocompatible fluorescent nanomaterials as mitochondrial targeting and blood-brain barrier penetrating biomarkers. *J Colloid Interface Sci* **2021,** *592*, 485-497.
13. Yan, X., Zhao, Y., Luo, J., Xiong, W., Liu, X., Cheng, J., Wang, Y., Zhang, M., Qu, H., Hemostatic bioactivity of novel Pollen Typhae Carbonisata-derived carbon quantum dots. *J Nanobiotechnology* **2017,** *15* (1), 60.
14. Zhang, M., Zhao, Y., Cheng, J., Liu, X., Wang, Y., Yan, X., Zhang, Y., Lu, F., Wang, Q., Qu, H., Novel carbon dots derived from Schizonepetae Herba Carbonisata and investigation of their haemostatic efficacy. *Artif Cells Nanomed Biotechnol* **2018,** *46* (8), 1562-1571.
15. Wang, Y., Kong, H., Liu, X., Luo, J., Xiong, W., Zhu, Y., Zhang, Y., Zhang, Y., Zhao, Y., Qu, H., Novel Carbon Dots Derived from Cirsii Japonici Herba Carbonisata and Their Haemostatic Effect. *J Biomed Nanotechnol* **2018,** *14* (9), 1635-1644.
16. Zhang, M., Cheng, J., Zhang, Y., Kong, H., Wang, S., Luo, J., Qu, H., Zhao, Y., Green synthesis of Zingiberis rhizoma-based carbon dots attenuates chemical and thermal stimulus pain in mice. *Nanomedicine (Lond)* **2020,** *15* (9), 851-869.
17. Kong, H., Zhao, Y., Zhu, Y., Xiong, W., Luo, J., Cheng, J., Zhang, Y., Zhang, M., Qu, H., Zhao, Y., Carbon dots from Artemisiae Argyi Folium Carbonisata: strengthening the anti-frostbite ability. *Artif Cells Nanomed Biotechnol* **2021,** *49* (1), 11-19.
18. Kucharzik, T., Koletzko, S., Kannengiesser, K., Dignass, A., Ulcerative Colitis-Diagnostic and Therapeutic Algorithms. *Dtsch Arztebl Int* **2020,** *117* (33-34), 564-574.
19. Wang, X., Zhang, Y., Kong, H., Cheng, J., Zhang, M., Sun, Z., Wang, S.,Liu, J., Qu, H., Zhao, Y., Novel mulberry silkworm cocoon-derived carbon dots and their anti-inflammatory properties. *Artif Cells Nanomed Biotechnol* **2020,** *48* (1), 68-76.
20. Zhao, Y., Zhang, Y., Kong, H., Zhang, M., Cheng, J., Luo, J., Zhao, Y., Qu, H., Haemostatic Nanoparticles-Derived Bioactivity of from Selaginella tamariscina Carbonisata. *Molecules* **2020,** *25*

(3).

21. Wilks S. Morbid appearances in the intestine of Miss Bankes.London Med Times Gazette. 1859,2:264.
22. Feuerstein, J. D., Moss, A. C., Farraye, F. A., Ulcerative Colitis. *Mayo Clin Proc* **2019,** *94* (7), 1357-1373.
23. Porter, R. J., Kalla, R., Ho, G. T., Ulcerative colitis: Recent advances in the understanding of disease pathogenesis. *F1000Res* **2020,** *9*.
24. Tatiya-Aphiradee, N., Chatuphonprasert, W., Jarukamjorn, K., Immune response and inflammatory pathway of ulcerative colitis. *J Basic Clin Physiol Pharmacol* **2018,** *30* (1), 1-10.
25. Agrawal, M., Prathyusha, E., Ahmed, H., Dubey, S. K., Kesharwani, P., Singhvi, G., Naidu, V. G. M., Alexander, A., Biomaterials in treatment of Alzheimer's disease. *Neurochem Int* **2021,** *145*, 105008.
26. Gao, Z., Shen, G., Zhao, X., Dong, N., Jia, P., Wu, J., Cui, D., Zhang, Y., Wang, Y., Carbon dots: a safe nanoscale substance for the immunologic system of mice. *Nanoscale Res Lett* **2013,** *8* (1), 276.
27. Pardo, J., Peng, Z., Leblanc, R. M., Cancer Targeting and Drug Delivery Using Carbon-Based Quantum Dots and Nanotubes. *Molecules* **2018,** *23* (2).
28. Henna, T. K., Pramod, K., Graphene quantum dots redefine nanobiomedicine. *Mater Sci Eng C Mater Biol Appl* **2020,** *110*, 110651.
29. Henna, T. K., Raphey, V. R., Sankar, R., Ameena Shirin, V. K., Gangadharappa, H. V., Pramod, K., Carbon nanostructures: The drug and the delivery system for brain disorders. *Int J Pharm* **2020,** *587*, 119701.
30. Xu, X., Zhang, K., Zhao, L., Li, C., Bu, W., Shen, Y., Gu, Z., Chang, B., Zheng, C., Lin, C., Sun, H., Yang, B., Aspirin-Based Carbon Dots, a Good Biocompatibility of Material Applied for Bioimaging and Anti-Inflammation. *ACS Appl Mater Interfaces* **2016,** *8* (48), 32706-32716.
31. Ge, G., Li, L., Wang, D., Chen, M., Zeng, Z., Xiong, W., Wu, X., Guo, C., Carbon dots: synthesis, properties and biomedical applications. *J Mater Chem B* **2021,** *9* (33), 6553-6575.
32. Tejwan, N., Saha, S. K., Das, J., Multifaceted applications of green carbon dots synthesized from renewable sources. *Adv Colloid Interface Sci* **2020,** *275*, 102046.
33. Zhang, M., Cheng, J., Sun, Z., Kong, H., Zhang, Y., Wang, S., Wang, X., Zhao, Y., Qu, H., Protective Effects of Carbon Dots Derived from Phellodendri Chinensis Cortex Carbonisata against Deinagkistrodon acutus Venom-Induced Acute Kidney Injury. *Nanoscale Res Lett* **2019,** *14* (1), 377.
34. Wu, J., Zhang, M., Cheng, J., Zhang, Y., Luo, J., Liu, Y., Kong, H., Qu, H., Zhao, Y., Effect of Lonicerae japonicae Flos Carbonisata-Derived Carbon Dots on Rat Models of Fever and Hypothermia Induced by Lipopolysaccharide. *Int J Nanomedicine* **2020,** *15*, 4139-4149.
35. Liu, Y., Zhang, M., Cheng, J., Zhang, Y., Kong, H., Zhao, Y., Qu, H., Novel Carbon Dots Derived from Glycyrrhizae Radix et Rhizoma and Their Anti-Gastric Ulcer Effect. *Molecules* **2021,** *26* (6).
36. Zhao, Y., Zhang, Y., Kong, H., Zhang, M., Cheng, J., Wu, J., Qu, H., Zhao, Y., Carbon Dots from Paeoniae Radix Alba Carbonisata: Hepatoprotective Effect. *Int J Nanomedicine* **2020,** *15*, 9049-9059.
37. Chassaing, B., Aitken, J. D., Malleshappa, M., Vijay-Kumar, M., Dextran sulfate sodium (DSS)-induced colitis in mice. *Curr Protoc Immunol* **2014,** *104*, 15.25.1-15.25.14.

38. Friedrich, M., Pohin, M., Powrie, F., Cytokine Networks in the Pathophysiology of Inflammatory Bowel Disease. *Immunity* **2019,** *50* (4), 992-1006.
39. Amirshahrokhi, K., Febuxostat attenuates ulcerative colitis by the inhibition of NF-κB, oinflammatory cytokines, and oxidative stress in mice. *Int Immunopharmacol* **2019,** *76*, 105884.
40. Niu, X., Zhang, H., Li, W., Wang, Y., Mu, Q., Wang, X., He, Z., Yao, H., Protective effect of cavidine on acetic acid-induced murine colitis via regulating antioxidant, cytokine profile and NF-κB signal transduction pathways. *Chem Biol Interact* **2015,***239*, 34-45.

Figures

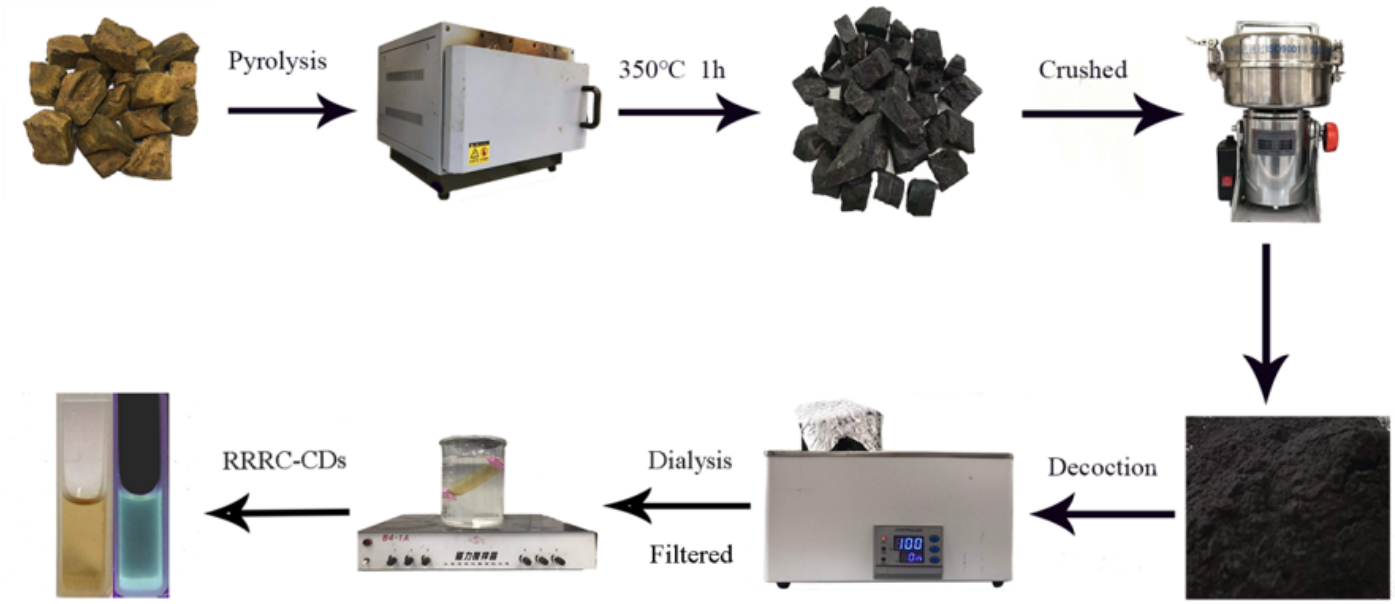

Figure 1

Preparation of Rhei radix et rhizoma-based carbon dots. The flowchart for the preparation process of carbon dots is derived from Rhei radix et rhizoma carbonisata.

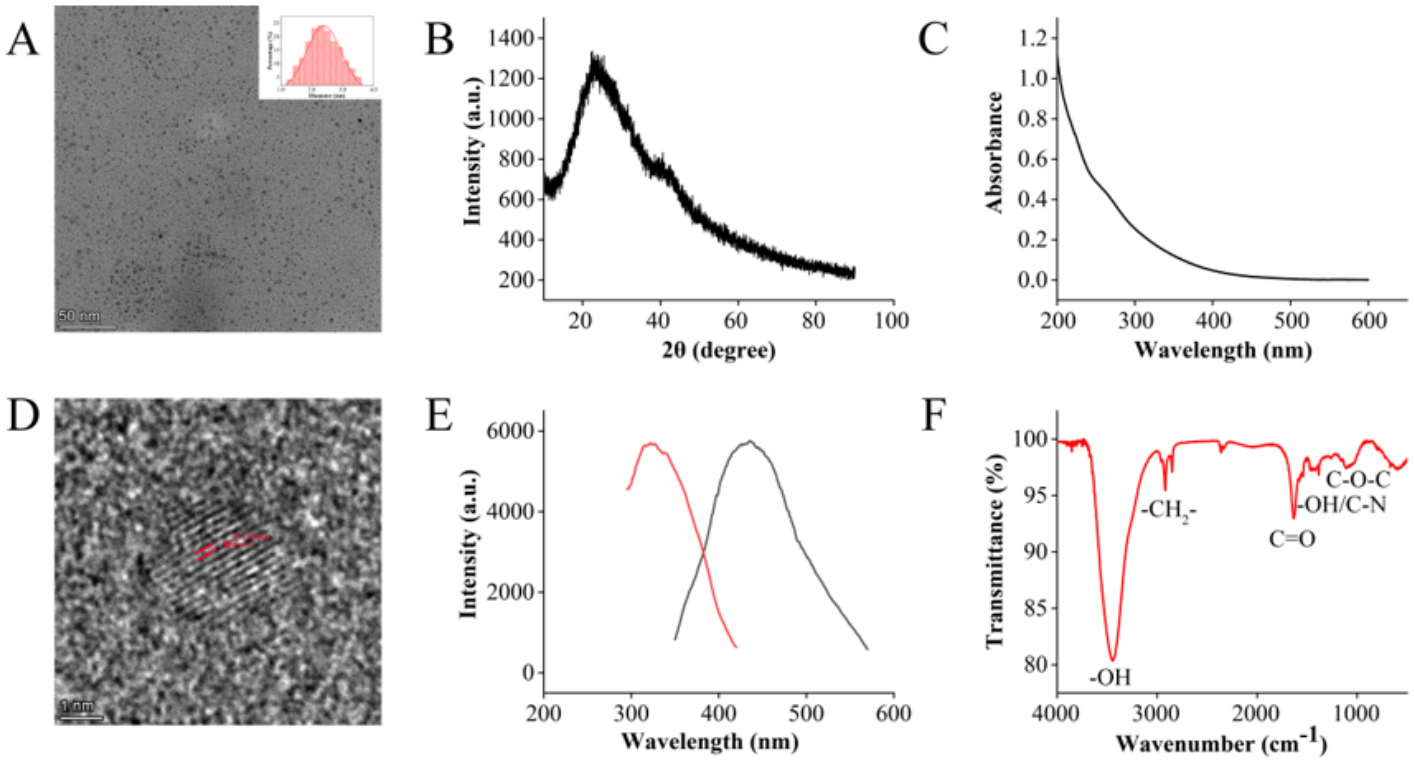

Figure 2

Characterization of Rhei radix et rhizoma carbonisata-derived carbon dots. (A) Low-resolution transmission electron microscope image. Inset: Histogram of particle size distribution. (B) XRD pattern. (C) Ultraviolet visible specturm. (D) High-resolution transmission electron microscope image. (E) Excitation and emission fluorescence spectra. (F) Fourier transform infrared spectroscopy.

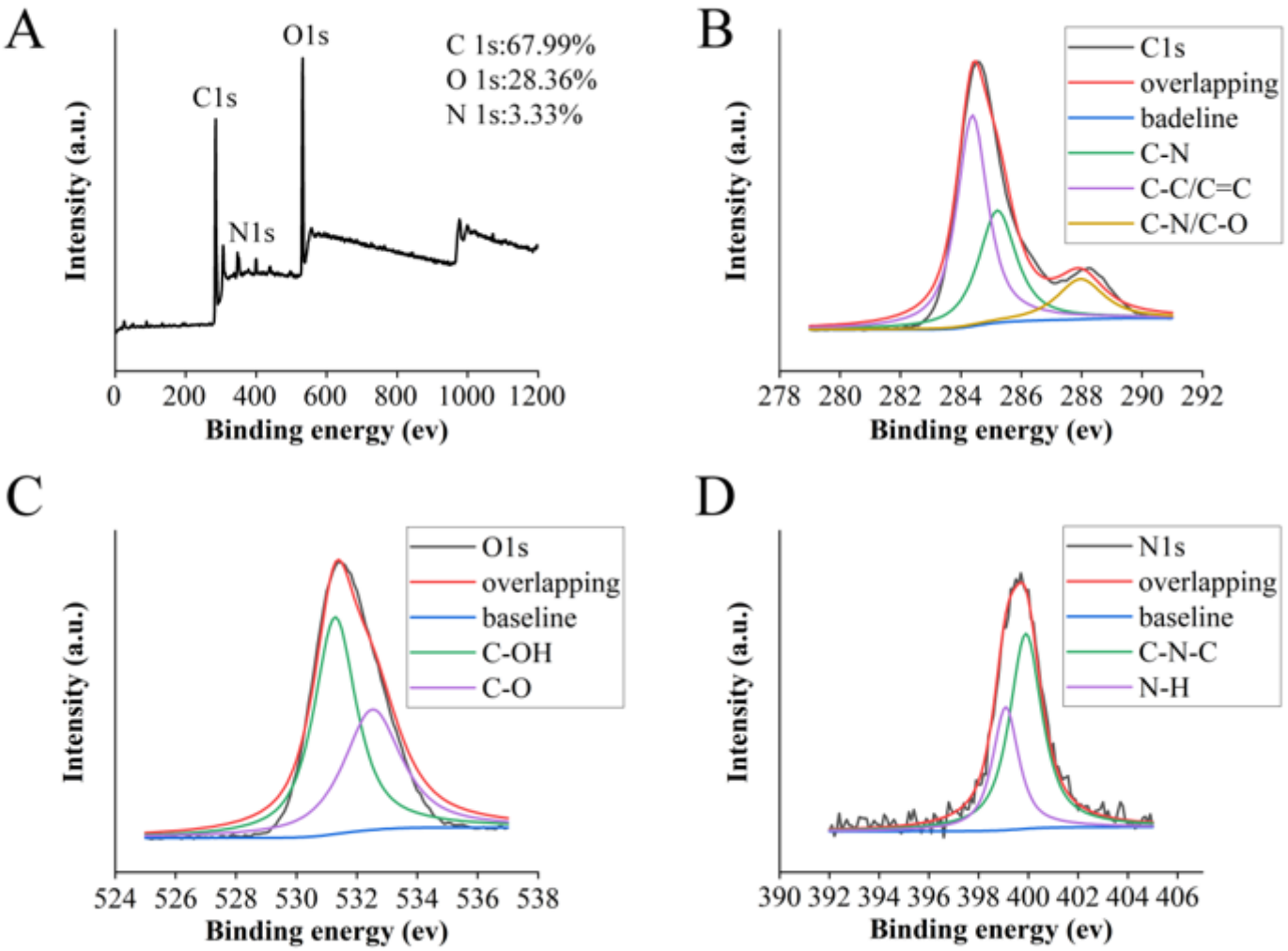

Figure 3

X-ray photoelectron spectroscopy of Rhei radix et rhizoma carbonisata-derived carbon dots. (A) Full-scan X-ray photoelectron spectrum of Rhei radix et rhizoma carbonisata-derived carbon dots. High-resolution measurement spectra of (B) C 1s, (C) O 1s, (D) N 1s.

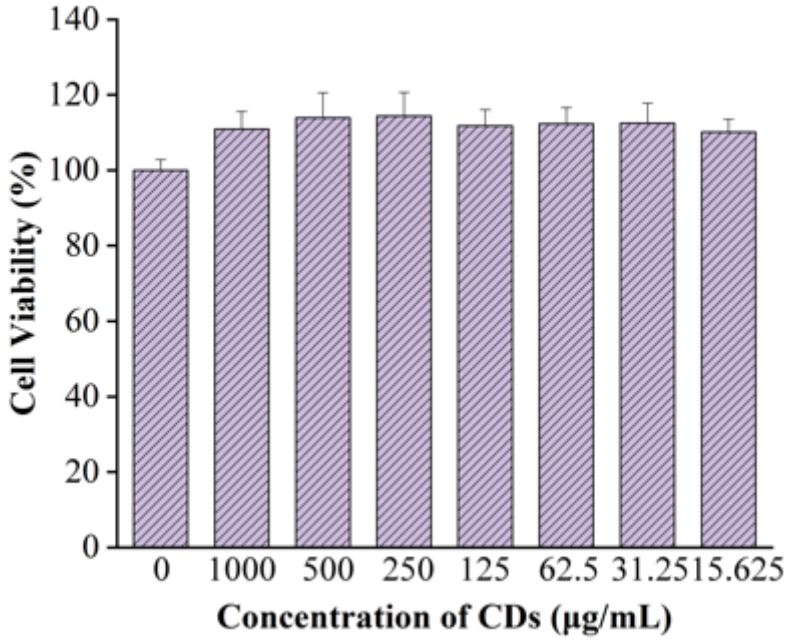

Figure 4

Cytotoxicity analysis in RAW cells treated with various doses of carbon dots derived from Rhei radix et rhizoma.

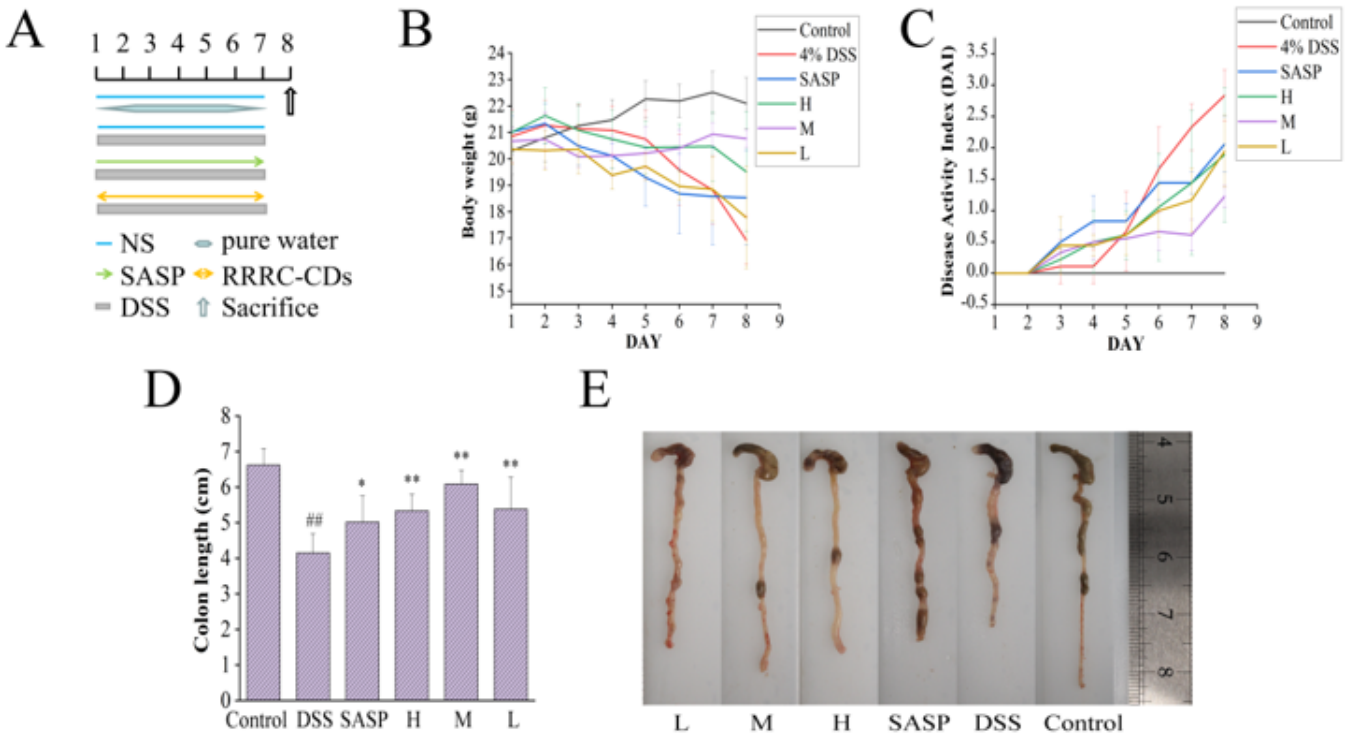

Figure 5

Effects of Rhei radix et rhizoma carbonisata-derived carbon dots on DSS-induced colitis in mice. (A) Experimental schedule of DSS-induced ulcerative colitis model in mice. (B) Body weight. (C) DAI score. (D) Colon length histogram. (E) Colon tissue photographs.

H, M, L: High-, Medium-, Low-dose (0.23, 0.12, and 0.06 mg/kg) RRRC-CD-administered groups, respectively.

Values are means ± SD, *p<0.05, **p<0.01 compared with the model group, $^{\#\#}$p<0.01 compared with the control group.

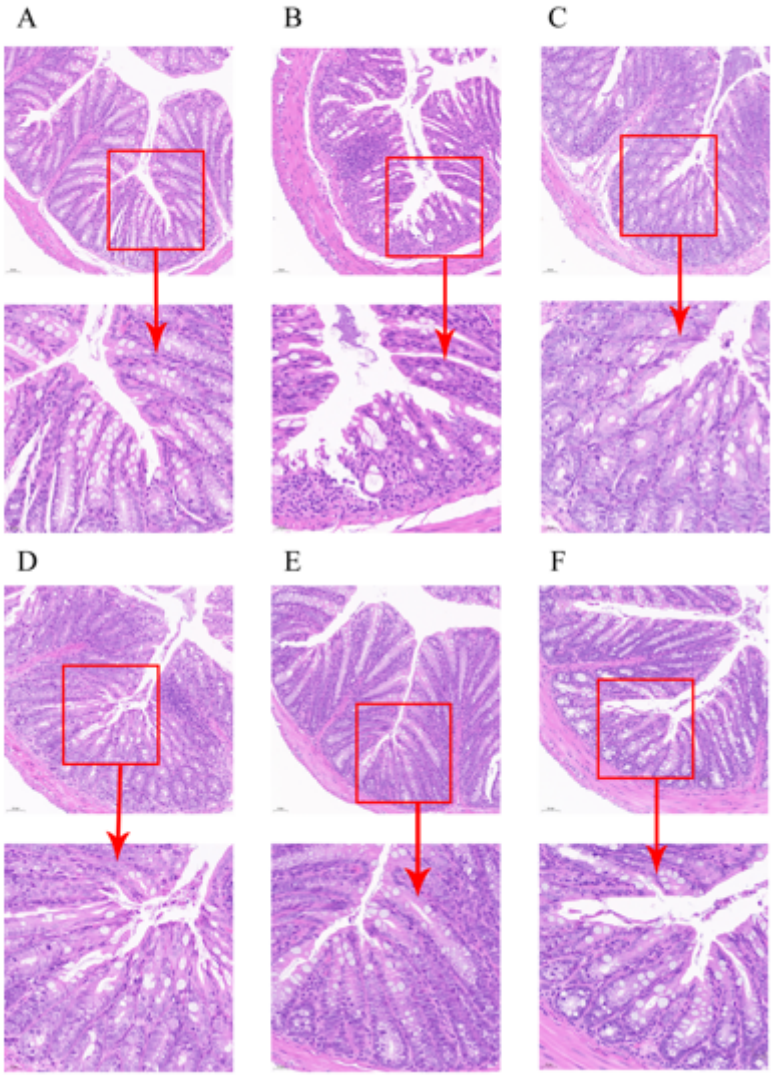

Figure 6

Rhei radix et rhizoma carbonisata-derived carbon dots ameliorate the histological changes of DSS-induced ulcerative colitis in mice. Histopathological sections of each group (A-F) were stained with H&E, scale bar = 50μm, 200×, 100μm, 400×.

(A) Control group. (B) Model group. (C) Positive group. (D) High-does group. (E) Mediun-dose group. (F) Low-dose group.

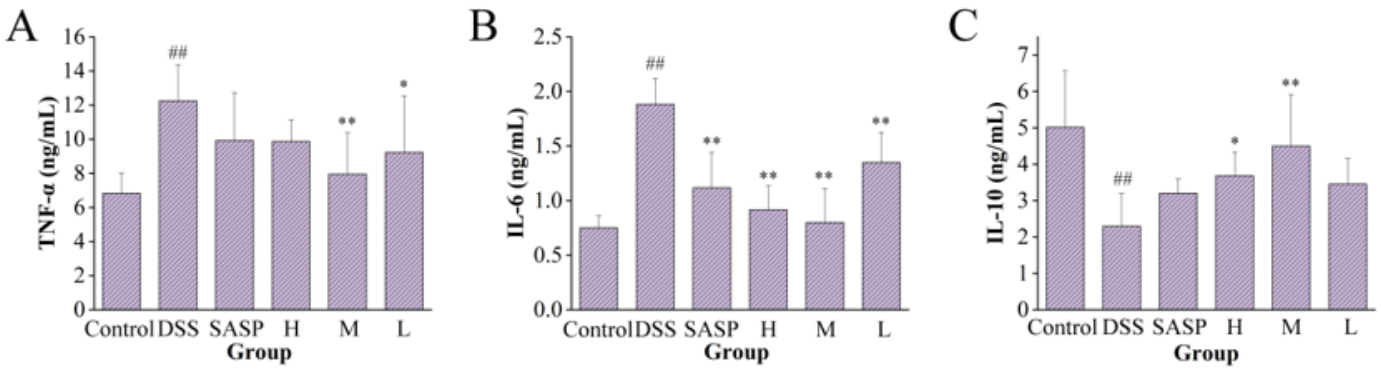

Figure 7

Effects of Rhei radix et rhizoma carbonisata-derived carbon dots on the level of TNF-α, IL-6, IL-10 in colon tissue. Mice were treated with NS, SASP, and different concentrations of Rhei radix et rhizoma carbonisata-derived carbon dots (H:0.23, M:0.12, L:0.06 mg/kg).

##p<0.01 compared with the control group, *p<0.05, **p<0.01 compared with the model group. Values are means ± SD.

H: High dose, M: Medium dose, L: Low dose.

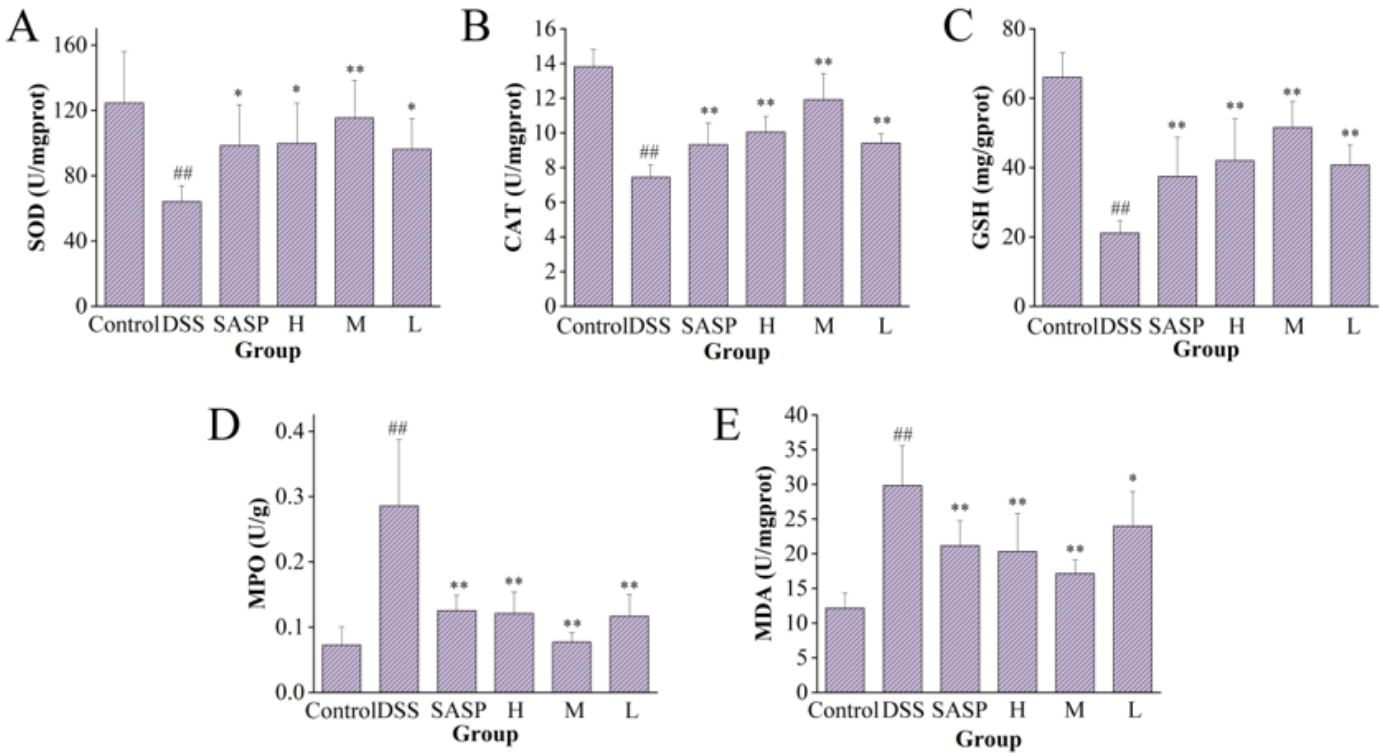

Figure 8

Effects of Rhei radix et rhizoma carbonisata-derived carbon dots on the level of SOD, CAT, GSH, MPO, MDA in colon tissue. Mice were treated with NS, SASP, and different concentrations of Rhei radix et rhizoma carbonisata-derived carbon dots (H:0.23, M:0.12, L:0.06 mg/kg).

##p<0.01 compared with the control group, *p<0.05, **p<0.01 compared with the model group. Values are means ± SD.

H: High dose, M: Medium dose, L: Low dose.